KL_4 Peptide Induces Reversible Collapse Structures on Multiple Length Scales in Model Lung Surfactant

Niels Holten-Andersen,[†] J. Michael Henderson,[†] Frans J. Walther,[‡§] Alan J. Waring,[‡¶‖] Piotr Ruchala,[¶] Robert H. Notter,[**††] and Ka Yee C. Lee[†*]

[†]Department of Chemistry, Institute for Biophysical Dynamics, and the James Franck Institute, University of Chicago, Chicago, Illinois; [‡]Los Angeles Biomedical Research Institute at Harbor-UCLA Medical Center, Torrance, California; [§]Department of Pediatrics, Leiden University Medical Center, Leiden, The Netherlands; [¶]Department of Medicine, School of Medicine, University of California, Los Angeles, California; [‖]Department of Physiology and Biophysics, School of Medicine, University of California, Irvine, California; [**]Department of Pediatrics and [††]Department of Environmental Medicine, University of Rochester School of Medicine, Rochester, New York

ABSTRACT We investigated the effects of KL_4, a 21-residue amphipathic peptide approximating the overall ratio of positively charged to hydrophobic amino acids in surfactant protein B (SP-B), on the structure and collapse of dipalmitoylphosphatidylcholine and palmitoyl-oleoyl-phosphatidylglycerol monolayers. As reported in prior work on model lung surfactant phospholipid films containing SP-B and SP-B peptides, our experiments show that KL_4 improves surfactant film reversibility during repetitive interfacial cycling in association with the formation of reversible collapse structures on multiple length scales. Emphasis is on exploring a general mechanistic connection between peptide-induced nano- and microscale reversible collapse structures (silos and folds).

INTRODUCTION

The development of a molecular thin film that remains stable during dynamic changes in area at the air-water interface of the lungs was a critical step in the evolution of air-breathing vertebrates (1–3). The air-water interface in the breathing lung needs to be stabilized to prevent alveolar collapse during exhalation, and to minimize work during inhalation (4–6). A material that serves this function began evolving hundreds of millions of years ago with the development of air-breathing vertebrates, resulting in the lipid-protein-based functional surfactant that coats the alveolar lining of the vertebrate lung today (1,3,7). Endogenous lung surfactant (LS) varies somewhat in composition among vertebrates, but consists predominantly of lipids with a small but functionally critical fraction of proteins (~7–10 wt%) (for a detailed review of surfactant composition see Notter (6)). Zwitterionic phosphatidylcholines make up 75–80% of surfactant phospholipids. The most prevalent single compound is dipalmitoylphosphatidylcholine (DPPC), but multiple additional saturated and unsaturated phosphatidylcholines are also present. LS also contains anionic phospholipids, with phosphatidylglycerol being the most prevalent anionic class in mature human lungs. LS proteins (SP-A through -D) are highly conserved in air-breathing vertebrates, surfactant proteins B (SP-B) and C (SP-C) have been demonstrated to be crucial in interacting with surfactant lipids to enhance the LS surface active function (3,6,8).

In accordance with its function in the lung, extracted LS dramatically increases surface pressure (π) when compressed on an aqueous subphase in surface balance experiments. The material also respreads rapidly during subsequent expansion without having experienced significant loss to the subphase (9). This physiologically crucial reversible compressibility is in large part possible due to unique material relaxations, observed as plateaus in π-area isotherms, which take place when the surfactant film is compressed beyond the maximum in-plane packing density (10). A plateau in π ~40 mN/m during compression of LS is caused by a structural collapse on the nanoscale via exclusion of disc-shaped structures enriched in lipids with lower collapse pressures from the monolayer (9). The discs range from 50 to 300 nm in diameter and 5 to 10 nm in height, and have been coined nanosilos (11). The nanosilos remain attached to the monolayer at $\pi > 40$ mN/m and reincorporate fully into the monolayer during expansion (12). At maximum compression (π near 72 mN/m, surface tension approaching zero) LS undergoes an out-of-plane relaxation on the microscale by folding into the subphase (9,13,14). The folds, several hundred microns long, tens of microns wide, and several microns deep, remain attached to the interface and are reversibly reincorporated back into the monolayer upon expansion (13,14).

Despite the importance of these nano- and microscale reversible collapse events to the performance of LS, any functional mechanistic connection between the two remains unexplored (15). However, because SP-B is known to play a central role in both the formation of nanosilos and in the promotion of micron-sized reversible folds in LS monolayers (11,13,16,17), the two are likely connected. Furthermore, of all the LS proteins, SP-B deficiency alone leads to lethal respiratory failure in preterm infants (18,19). Hence, the identification of a functional mechanism that connects these multiple length scale reversible collapse events in

Submitted June 6, 2011, and accepted for publication October 6, 2011.

*Correspondence: kayeelee@uchicago.edu

Editor: Paulo F. Almeida.

0006-3495/11/12/2957/9 $2.00

doi: 10.1016/j.bpj.2011.10.050

LS is undoubtedly vital for the design of synthetic surfactants that successfully mimic native function.

Since the first demonstration of the importance of SP-B in surfactant activity, the search for synthetic peptides mimicking its function has been ongoing, driven both by a desire to find a cheaper and purer alternative to animal-derived surfactant preparations and by concern over their inherent risk of zoonotic infection such as prion transmission (e.g., bovine spongiform encephalitis) (6,20,21). KL_4, a 21-residue peptide containing repeating KLLLL subunits, represents one of the early synthetic surfactant peptides designed to roughly reflect the overall ratio of cationic to hydrophobic amino acids found in native SP-B (22). Despite an early demonstration of SP-B-like activity and the fact that KL_4 is currently under evaluation for FDA approval for clinical use as the peptide component of the synthetic exogenous surfactant Surfaxin (Lucinactant), surprisingly little is known about the specific effects of KL_4 on phospholipid interfacial film behavior during compression/expansion and collapse (23,24).

Using KL_4 peptide along with zwitterionic DPPC and anionic palmitoyl-oleoyl-phosphatidylglycerol (POPG) lipids as model LS components, we explore the potential mechanistic connection between nanosilos and reversible folding of surfactant monolayers. We demonstrate that the presence of KL_4-induced nanosilos correlates with increased reversible folding of monolayers and discuss how KL_4, despite its primitive molecular similarity with SP-B, induces similar monolayer mechanics.

EXPERIMENTAL SECTION

Materials

Peptide synthesis reagents were purchased from AnaSpec (San Jose, CA), HPLC solvents from Fisher Scientific (Pittsburgh, PA), and all other chemicals from Sigma (St. Louis, MO) and Aldrich (Milwaukee, WI). DPPC and POPG were obtained in powder form from Avanti Polar Lipids (Alabaster, AL) and used without further purification. For all Langmuir trough experiments, the fluorescent probe used for visualization with fluorescence microscopy (FM) was Texas Red-labeled 1,2-dihexadecanoyl-*sn*-glycerol-3-phosphoethanolamine (TR-DHPE; Molecular Probes, Eugene, OR). The subphase was ultrapure water (resistivity ≥ 18 MΩ-cm) processed by a Milli-Q ultrapurification system (A-10 gradient, Millipore, Bedford, MA). Because experiments were performed on monolayers containing POPG, ultrahigh purity Argon 5.0 (Airgas) was used to minimize oxidative damage to the unsaturated oleoyl chain.

Synthesis of KL_4 peptide

KL_4 peptide (KL_4-UCLA) was prepared with either an ABI 431A solid phase peptide synthesizer (Applied Biosystems, Foster City, CA) configured for FastMoc chemistry (25), a Symphony Multiple Peptide Synthesizer (Protein Technologies, Tucson, AZ) using standard Fmoc synthesis, or a Liberty Microwave Peptide Synthesizer (CEM, Matthews, NC) configured for standard Fmoc synthesis. A low substitution (0.43 mmole/gm) pre-derivatized Fmoc-Lys(Boc)-Wang resin (NovaBiochem, San Diego, CA) was employed for synthesis of the KL_4 peptide. All residues were double-coupled to insure optimal yield. After synthesis of the sequence, peptide was cleaved and deprotected from the resin using a mixture of 0.75 gm phenol, 0.25 ml ethanedithiol, 0.5 ml of thioanisole, 0.5 ml of deionized water, and 10 ml trifluoroacetic acid per gram of resin initially chilled to 5°C, and then allowed to come to 25°C with continuous shaking over a period of 2 h to insure complete peptide deprotection (26). Crude peptide was removed from the resin by vacuum-assisted filtration of the resin in a 0.5 mmole Rainin style reaction vessel (AnaSpec, Fremont, CA), with trifluoroacetic acid and dichloromethane. The filtered crude peptide was precipitated in ice-cold tertiary butyl ether, and separated by centrifugation at 2000 $\times$ *g* for 10 min (2–3 cycles of ether precipitation and centrifugation were used to minimize cleavage-deprotection byproducts). Reduced crude peptides from ether precipitation were verified for molecular mass by MALDI-TOF spectroscopy, dissolved in trifluoroethanol:10 mM HCl (1:1 v:v), freeze-dried, and purified by preparative HPLC (26).

Lateral compression experiments

The experimental protocol has been described previously (12). Briefly, monolayer spreading solutions of DPPC, POPG, or DPPC/POPG (7:3 molar ratio) were prepared by dissolving in chloroform (HPLC grade, Fisher Scientific) at a concentration of 0.1 mg/ml and adding 0.5 mol% of TR-DHPE. KL_4 peptide was dissolved in methanol and added to the lipid solutions before spreading. Peptide concentrations investigated were 4, 8, or 16 wt% relative to phospholipid to allow maximum effects to be discerned and elucidated. Peptide concentrations were confirmed using amino acid analysis (Keck Biotechnology Resource Laboratory, Yale University, New Haven, CT). Lipid solutions were stored at −20°C in glass vials. All experiments were performed at 25°C on pure water. Monolayers were spread at the gas/water interface of a Langmuir trough (see below) by gently depositing drops of the spreading solution onto the surface, and the organic solvent was allowed to evaporate for at least 20 min. The barriers were then compressed at 0.1 mm/s, and isotherm measurements were obtained at 1-s intervals in the form of surface pressure π (mN/m) ($\pi = \gamma_o - \gamma$, where γ_o is the surface tension of pure water at the experimental temperature and γ is the surface tension when the surfactant film is present) versus area per lipid molecule (Å^2/molecule). The surface was imaged continuously with FM throughout compression. All experiments were done at least three times to ensure reproducibility. Representative data are shown in the results.

Langmuir trough and FM methods

The Langmuir trough setup was as previously described (12). Briefly, it consisted of a custom-made Teflon trough equipped with two Teflon barriers whose motions were controlled by a pair of translational stages (UTM100, Newport, Irvine, CA) for symmetric compression or expansion. A stationary Wilhelmy slide (Riegler and Kirstein, Berlin, Germany) was used to measure surface pressure as surface area was reduced (compression) or increased (expansion). Subphase temperature during cycling was maintained at 25 $\pm$ 0.5°C with a home-built control station composed of thermoelectric units (Marlow Industries, Dallas, TX) joined to a heat sink held at 20°C by a Neslab RTE-100 water circulator (Portsmouth, NH). A piece of resistively heated cover glass (Delta Technologies, Dallas, TX) was placed over the trough and held at a higher temperature to suppress evaporative losses, minimize convective currents, and prevent water condensation on the objective. The assembly was fixed to a custom-built microscope stage to allow simultaneous FM with $\times$20 and $\times$50 extra-long working distance objectives (Nikon Y-FL, Fryer, Huntley, IL). A high-pressure mercury lamp (Osram Sylvania, Danvers, MA) was used for fluorescence excitation and the emitted light was gathered with a dichroic mirror/filter cube (Nikon HYQ Texas Red, Fryer). Images were collected at 30 frames/s using a charge-coupled device camera (Stanford Photonics, Palo Alto, CA), and recorded via a digital video recorder (Sony, B&H Photo-Video, New York, NY). The entire assembly

is mounted on a vibration isolation table (Newport) and controlled by a custom software interface written using LabView 6.1 (National Instruments, Dallas, TX).

Atomic force microscopy

Submicron resolution images of various compositional monolayers transferred from the gas/water interface were obtained with atomic force microscopy (AFM). Monolayers were isothermally compressed to 50 mN/m and transferred onto a mica substrate by an inverse Langmuir-Schaefer transfer technique previously described (27). Briefly, a freshly cleaved mica substrate (Hi-grade V2 mica, Ted Pella, Redding, CA) epoxied to a magnetic stainless steel disc (15 mm diameter, Ted Pella) was placed into a stainless steel apparatus with a surrounding 2 mm high machined knife edge, and the entire setup was placed on the bottom of the trough before the start of the experiment and remained submerged in the subphase throughout the compression isotherm. At the desired surface pressure, the subphase was slowly aspirated to lower the subphase level to the point when the knife edge cut the monolayer, thus preserving the surface pressure and the morphology of the transferred film. Drilled holes at the bottom of the steel piece allowed water to exit the chamber completely until the monolayer was deposited on the mica. Monolayer morphology before, during, and after transfer was monitored with FM to ensure that the transfer process did not perturb the integrity of the film.

Transferred monolayers were imaged at ambient temperature in air using a Multimode Nanoscope IIIA scanning probe microscope (Digital Instruments, Santa Barbara, CA) with a Type J scanner in contact mode. Cantilevers having a nominal spring constant of 0.32 N/m with sharpened silicon nitride tips (NP-S, Veeco Probes, Camarillo, CA) were used. The tips were decontaminated by ultraviolet-generated ozone before sampling (PSD-UV Surface Decontamination System, Novascan, Ames, IA). A deflection setpoint of zero volts was used during imaging to minimize contact forces and hence film damage. Micrographs were obtained at a scan rate of 1.0 Hz at a resolution of 512 pixels/line. To improve image clarity, AFM scans covering a linear dimension of 50 μm were subjected to a second-order flattening procedure to compensate for sample tilt and bow between each scan line, whereas high resolution scans covering 5 μm were subjected to a first-order flattening procedure to compensate for sample tilt alone (raised features were excluded from the flattening calculation).

RESULTS

Fig. 1 *A* shows the isotherms of three compression-expansion cycles of a DPPC monolayer at 25°C. Two plateaus are discernible in the isotherms: one at ~10 mN/m, signifying the coexistence of the liquid expanded and the condensed phase, and another at ~72 mN/m pointing to monolayer collapse, i.e., where the film is no longer stable in two dimensions and starts sampling the third dimension. FM images of DPPC at high surface pressure reveal a film made up of mainly dark (dye excluded) domains, signifying a highly condensed film. Such a film collapses by a fracture-like mechanism (Fig. 1 *A* and (15)), which results in poor respreading during expansion and low reversibility in repeated cycling, as demonstrated by the hysteresis in the isotherms. Pure POPG monolayers display very poor reversibility in repeated compression-expansion (Fig. 1 *B*). The fluid state of POPG prevents any in-plane condensation during compression; hence, its isotherm only shows a single plateau at collapse. Its more fluid nature also results in its

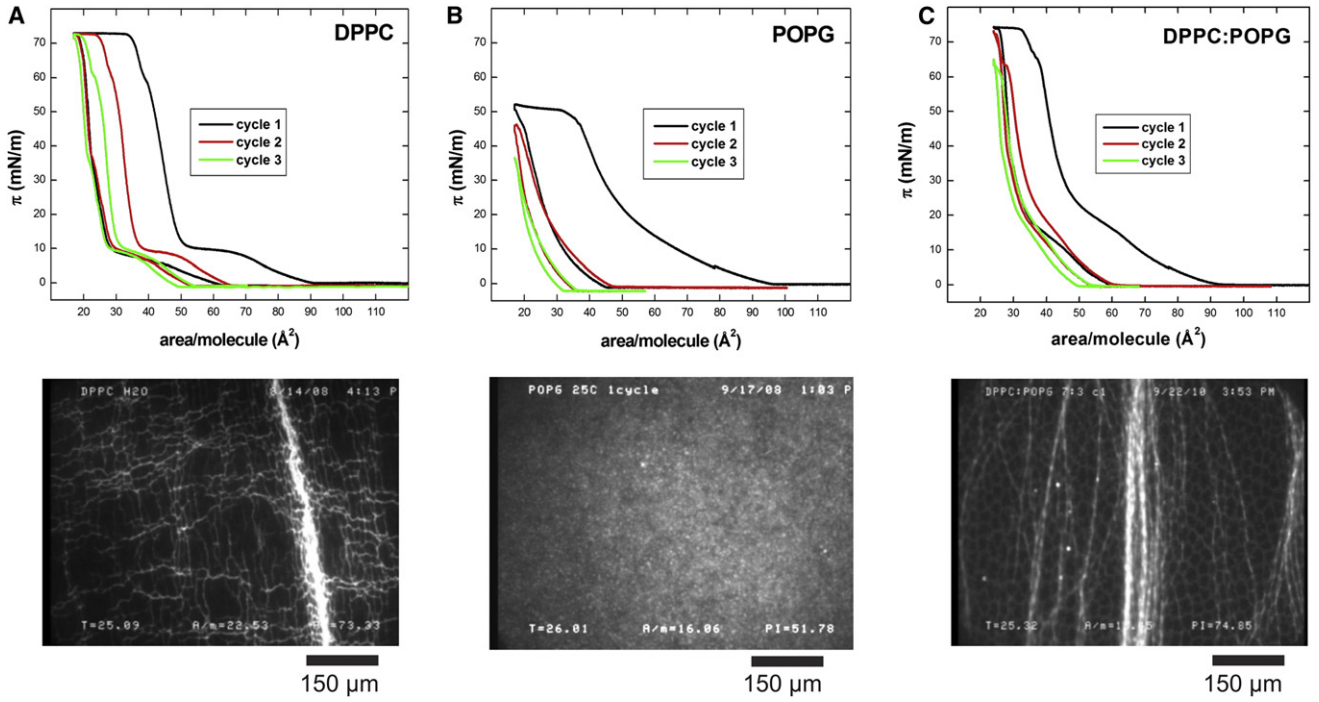

FIGURE 1 (*A*) Isotherms of a DPPC monolayer during repeated compression (*3 curves to the right*) and expansion (*3 curves to the left*) at 25°C. FM image below shows a highly condensed (*dark*) film at high pressure that eventually undergoes a fracture-like collapse at maximum compression (*image from 1st cycle*). (*B*) Isotherms of a POPG monolayer during repeated compression and expansion at 25°C. FM image below shows a fluid (*bright*) film with no condensed domains that undergoes vesicular collapse at maximum compression (*image from 1st cycle*). (*C*) Isotherms of a DPPC/POPG (7:3) monolayer during repeated compression and expansion at 25°C. FM image below shows the folding collapse at maximum compression (*image from 1st cycle*).

lower resistance against lateral compression, resulting in a lower collapse pressure (~50 mN/m) compared to that of DPPC. At collapse, POPG gets excluded from the monolayer, forming vesicles (see *bright structures in FM image* of Fig. 1 *B*) that go into the subphase. Collapse results in a large loss of material that cannot be reincorporated into the monolayer in subsequent cycles (see *isotherms* in Fig. 1 *B*). Adding 30 mol% of the fluid POPG to DPPC decreases the sharpness of the plateau at ~10 mN/m and signifies the onset of nucleation of the condensed DPPC phase, which gives rise to a biphasic monolayer with dark DPPC condensed domains sitting in a bright, fluid POPG matrix (see *FM image* in Fig. 1 *C*) (15). The addition of POPG also changes the monolayer collapse mechanism to folding (see *FM image* in Fig. 1 *C*); however, the overall reversibility of the monolayer remains poor due to POPG loss to the subphase (15,28,29).

Adding 8 wt% KL_4 to DPPC/POPG (7:3) noticeably changes the resulting folding collapse of the monolayer at π near 72 mN/m (see *FM image* in Fig. 2 *A*). The folds now display significantly increased reincorporation upon expansion (see Fig. 2 *D*), which improves reversibility during cycling (see *isotherms* in Fig. 2 *A*). An additional plateau at π ~40 mN/m is also apparent when KL_4 is present. To discern whether this change in collapse is due to the interaction of KL_4 with DPPC or POPG, we examined the effects of the addition of the peptide to pure POPG and pure DPPC monolayers. When KL_4 is added at 16 wt% to POPG, the resulting monolayer begins collapsing at π values slightly above 40 mN/m into disc-like structures with lateral dimensions from 100 nm to 10 μm (see *FM image* in Fig. 2 *B*). These discs are much larger in length scale than previously reported nanosilos (11,12), and are termed microsilos here. The collapse plateau of the POPG/KL_4 film (see *isotherms* in Fig. 2 *B*) is similar in pressure to that of the additional plateau in the isotherms observed for mixed DPPC/POPG monolayers when KL_4 is present (Fig. 2 *A*). The microsilo disc-like structures remain attached to the POPG/KL_4 monolayer during continued compression, and completely reincorporate back into the monolayer during expansion (see Fig. 2 *E*). In repeated compression-expansion cycles, the POPG/KL_4 monolayer accordingly displays increased reversibility (see *isotherms* in Fig. 2 *B*). Adding 16 wt% KL_4 to a pure DPPC monolayer, on the other hand, appears to suppress its tendency to collapse by fracture at π near 72 mN/m; however, it does not improve its reversibility (Fig. 2 *C*).

The π-A isotherm behavior of mixed DPPC/POPG (7:3) monolayers containing differing contents of KL_4 (4, 8, 16 wt% peptide) is shown in Fig. 3, *A* and *B*. High compression folding collapse of all DPPC/POPG (7:3) films containing KL_4 occurs at π near 72 mN/m, with the isotherm plateau during compression at π ~40 mN/m becoming more prominent as peptide concentration increases. In mixed DPPC/POPG (7:3) monolayers, KL_4 induces the formation of nano- rather than microsilos at the plateau at ~40 mN/m. Dependent on the KL_4 concentration, the fluid matrix (*bright region between condensed dark domains in fluorescence micrographs*, see Fig. 3 *C*) sees an increase in number density, size, and height of nanosilos upon AFM inspection of transferred samples (see Fig. 3, *D* and *E*). For 4–16 wt% KL_4, the diameter of nanosilos ranges from 20 nm to 1 μm and the height from 5 to 50 nm, with a prevalence of larger structures at higher KL_4 contents. The increased amount of monolayer material incorporated into nanosilos at high KL_4 content revealed by AFM correlates with the length of the pressure plateau near 40 mN/m observed in π-A isotherms (Fig. 3 *A*). High concentrations of KL_4 in DPPC/POPG (7:3) monolayers also increase their overall reversibility on cycling (compare *isotherms* in Fig. 3 *B* at 16 wt% KL_4 with Fig. 2 *A* at 8 wt% KL_4).

Major π-A isotherm features for DPPC/POPG (7:3) films containing a high KL_4 concentration of 16 wt% are found to be traced with reasonable agreement by the combined isotherms of POPG + KL_4 (16 wt%) and DPPC/POPG (7:3) (Fig. 4 *A*). In particular, the features of the prominent isotherm compression plateau at π ~40 mN/m and the high pressure collapse at π near 72 mN/m are shown to be replicated by combining the separate isotherms. An increased amplitude of π oscillations is also apparent during folding collapse of DPPC/POPG (7:3) films with 16 wt% KL_4 in association with an increase in the size of folding collapse structures seen by FM (see *inset* in Fig. 4 *A* and *FM images* in *B*).

DISCUSSION

Our work shows that a simple synthetic surfactant peptide like KL_4 can similarly induce the formation of reversible silo structures like SP-B (Figs. 2 *B* and 3, *C–F*), during compression of monolayers containing phospholipids with unsaturated fatty acyl chains and negatively charged head groups, such as POPG. However, nanosilos shown here to be induced by KL_4 in mixed DPPC/POPG (7:3) monolayers (Fig. 3, *D–F*), display a slightly larger maximum diameter (up to 1 μm) and height (up to 50 nm) compared to those observed for monomeric or dimeric SP-B 1–25 peptides (up to 400 nm in diameter and 20 nm in height) at comparable peptide concentrations in DPPC/POPG films (11,12). Molecular differences between KL_4 and SP-B are well known (30–32), but how these might affect the formation of nanosilos or other collapse structures is unclear. The first 7–10 residues in the amino-terminal sequence of SP-B 1–25 (***FPIPLPYCWL***CRALIKRIQAMPIAMIPKG) have been identified as functioning at least in part as an insertion sequence, facilitating molecular penetration into lipid bilayers and monolayers (12,33,34). Frey et al. (12) have recently proposed that this N-terminal insertion sequence region plays an important role in stabilizing the edge of nanosilos modeled as POPG-enriched bicelles excluded

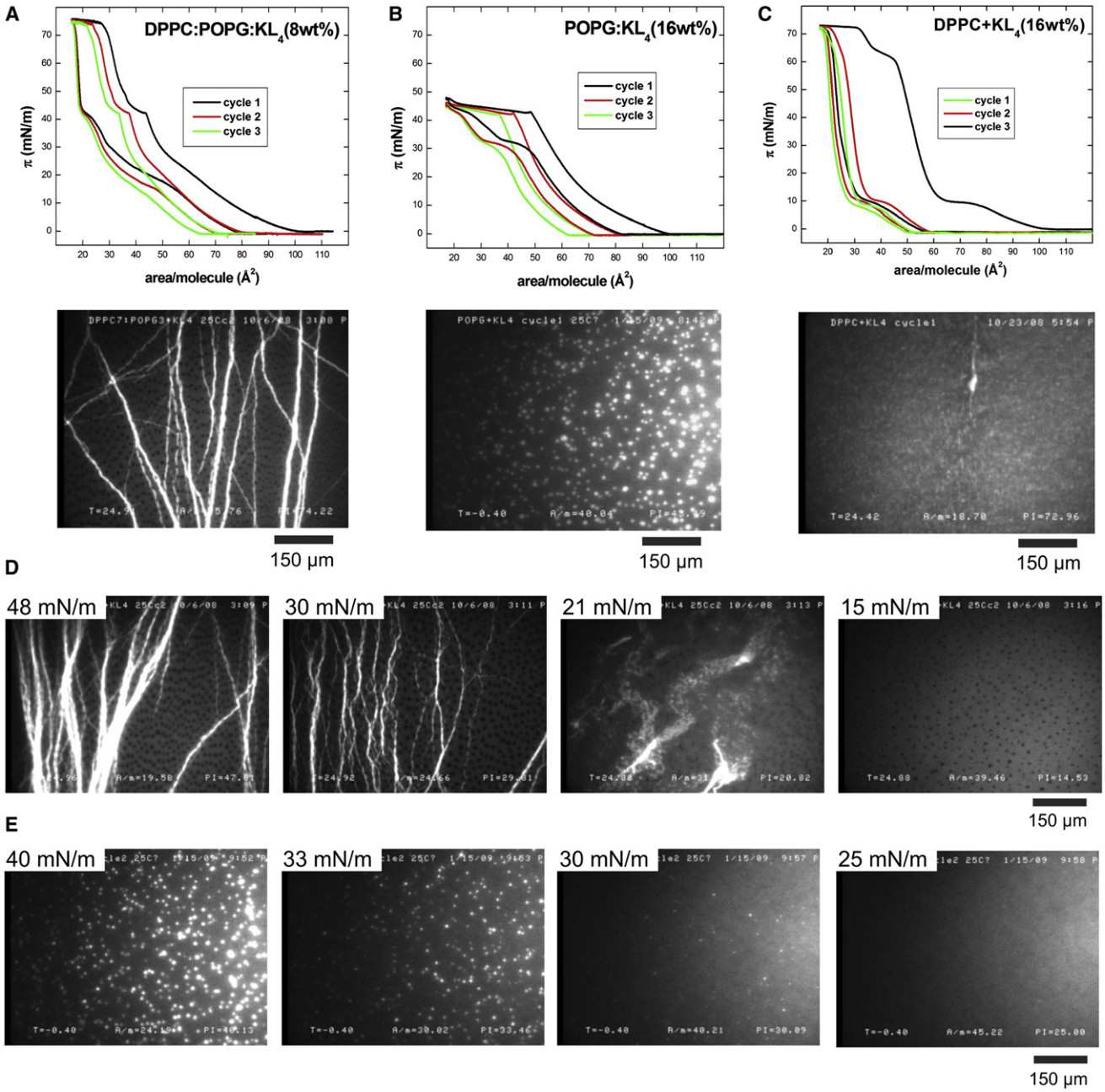

FIGURE 2 (*A*) Isotherms of a DPPC/POPG (7:3) monolayer with 8 wt% KL_4 during repeated compression (*3 curves to the right*) and expansion (*3 curves to the left*) at 25°C. FM image below shows the change in folding collapse at maximum compression induced by KL_4 (*image from 2nd cycle*). (*B*) Isotherms of a POPG monolayer with 16 wt% KL_4 during repeated compression and expansion at 25°C. FM image below shows the microsilo collapse at maximum compression (*image from 1st cycle*). (*C*) Isotherms of a DPPC monolayer with 16 wt% KL_4 during repeated compression and expansion at 25°C. FM image below shows the suppressed folding collapse at maximum compression induced by KL_4 (*image from 1st cycle*). (*D*) Series of FM images from the 2nd cycle showing the reincorporation of folds upon expansion of a DPPC/POPG (7:3) monolayer with 8 wt% KL_4. The surface pressure (π) during expansion is indicated in each image. (*E*) Series of FM images from the 2nd cycle showing the complete reincorporation of microsilos upon expansion of a POPG monolayer with 16 wt% KL_4. The surface pressure (π) during expansion is indicated in each image.

from the monolayer. This model is further supported by the observation that SP-B 1–25 reorients from a parallel to a perpendicular orientation with respect to the interface during compression of a PG-containing monolayer (35), thereby orienting the peptide in a configuration favorable to electrostatic and hydrophobic edge stabilization of excluded POPG bicelles. Frey et al. (12) reported incremental heights of nanosilos induced by SP-B 1–25 to be ~5 nm, consistent with stacks of POPG bilayers stabilized along the periphery by peptide. The height distribution of nanosilos induced by KL_4 in mixed DPPC/POPG (7:3) monolayers display similar discrete steps matching with

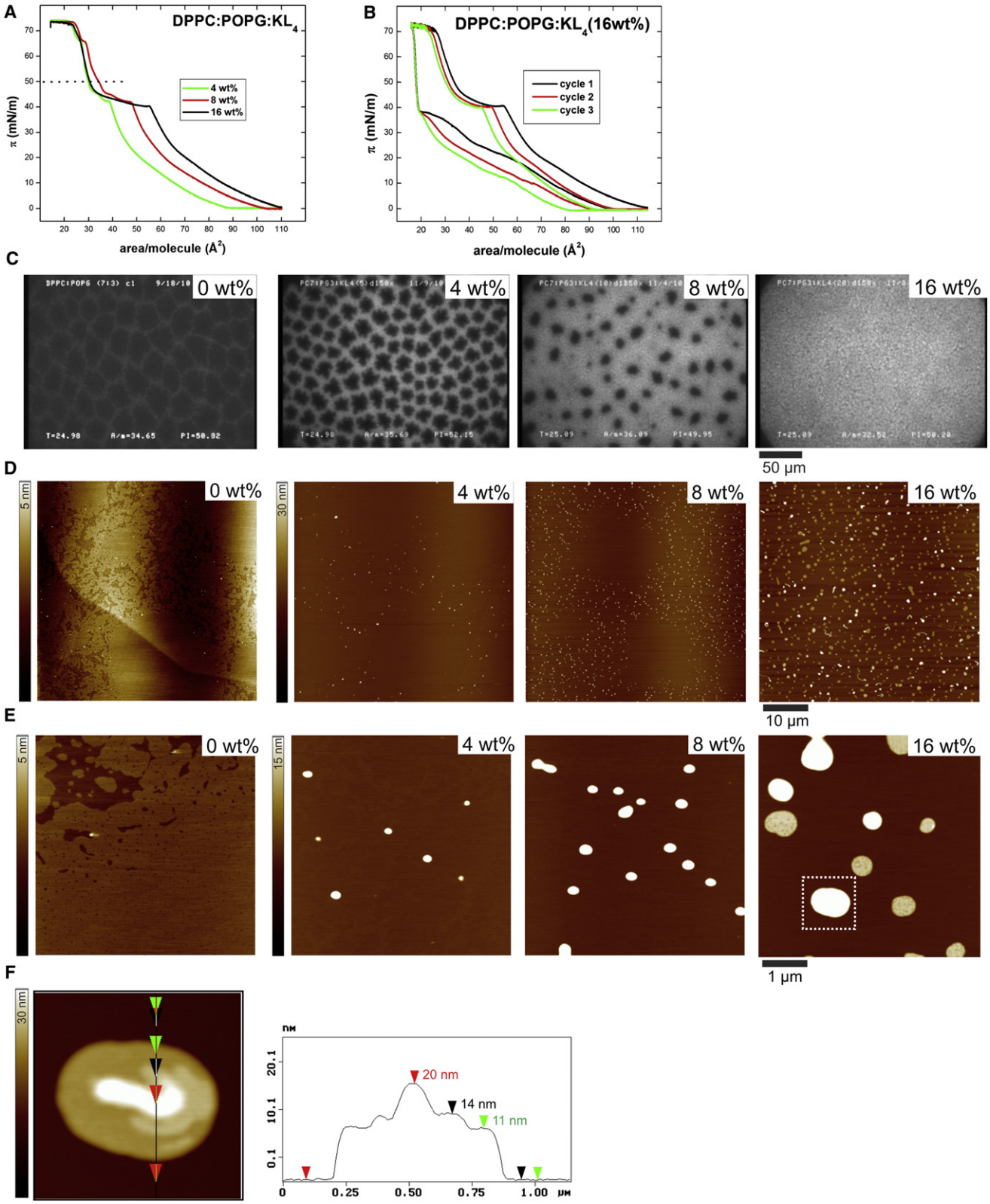

FIGURE 3 (*A*) Isotherms of a DPPC/POPG (7:3) monolayer with 4, 8, and 16 wt% KL_4 during compression at 25°C. Dashed line indicates pressure of monolayers inspected by FM and by AFM after deposition onto solid mica substrates. (*B*) Isotherms of a DPPC/POPG (7:3) monolayer with 16 wt% KL_4 during repeated cycles of compression (*3 curves to the right*) and expansion (*3 curves to the left*) at 25°C. (*C*) FM images of DPPC/POPG (7:3) monolayers with 0, 4, 8, and 16 wt% KL_4 at π ~50 mN/m. The dark regions are the DPPC-rich condensed domains and the bright regions the POPG-rich fluid matrix. With 16 wt% of KL_4, condensation is no longer visible in FM. (*D* and *E*) AFM images at 50 × 50 μm (*D*) and 5 × 5 μm (*E*) scan size of DPPC/POPG (7:3)

the thickness of POPG bicelles (Fig. 3 *F*). This suggests that, despite its lack of a dedicated insertion sequence and overall poor sequence similarity with SP-B, KL_4 is able to stabilize POPG bicelle silo structures via a combination of electrostatic and hydrophobic interactions as proposed for SP-B (23,24). Recent work by Long et al. (30) further demonstrates that KL_4 can switch from a parallel to a perpendicular orientation within POPG-enriched bilayers in support of a general SP-B mimetic behavior of KL_4. Further evidence that POPG/KL_4 interactions are responsible for the formation of reversible silo structures is provided by our observation that micro- or nanosilos, respectively, were induced at the same π near 40 mN/m in POPG and DPPC/POPG (7:3) monolayers (Figs. 2, *A* and *B* and 3, *A*, *D*, and *E*). The larger size of silos induced by KL_4 in pure fluid POPG monolayers compared to DPPC/POPG (7:3) films indicates that phospholipid molecular distribution affects the lateral length scale of peptide-induced silos.

The individual importance of reversible silo and folding structures in the LS monolayer function has been previously addressed separately. The idea that a functional connection exists across the length scales of the two types of collapse structures has not been explored but is supported by our data. First, the presence of nanosilos correlates with increased reversible folding in DPPC/POPG (7:3) monolayers containing KL_4 (Figs. 2 *A* and 3, *B*, *D*, and *E*). Second, several major features in the π-A isotherm of DPPC/POPG (7:3) with 16 wt% KL_4 can be retraced by the combined isotherms of POPG + KL_4 (16 wt%) and DPPC/POPG (7:3) (Fig. 4 *A*), which supports that, when present in monolayers, nanosilos directly contribute to increased reversible monolayer folding. Finally, the increased amplitude of π oscillations near 72 mN/m (see *inset* in Fig. 4 *A*) suggests that the presence of nanosilos in monolayers during folding collapse increases final fold size. These larger fold sizes are confirmed via FM (Fig. 4 *B*) and suggest an increased bending stiffness of the surfactant film because fold size (l) of thin elastic sheets has recently been shown by Pocivavsek et al (36) to scale as $l \sim B/K^{1/2}(1/\Delta)$, where B is bending stiffness, K is substrate stiffness, and Δ is relative compression. With water as our substrate, K remains constant throughout our experiments and only changes in the surfactant film that added to B will lead to increased l of the surfactant film during compression. Nanosilos could enhance B by modifying the intrinsic molecular distribution in the surfactant film and/or increase its thickness. For example, molecular reorganization caused by the mass transfer of POPG into the nanosilo repository could improve DPPC condensation and increase surfactant in-plane stiffness during compression (37). Additionally, the high packing density of nanosilos attached to the monolayer during the final stages of compression could effectively stiffen the surfactant film by increasing its thickness.

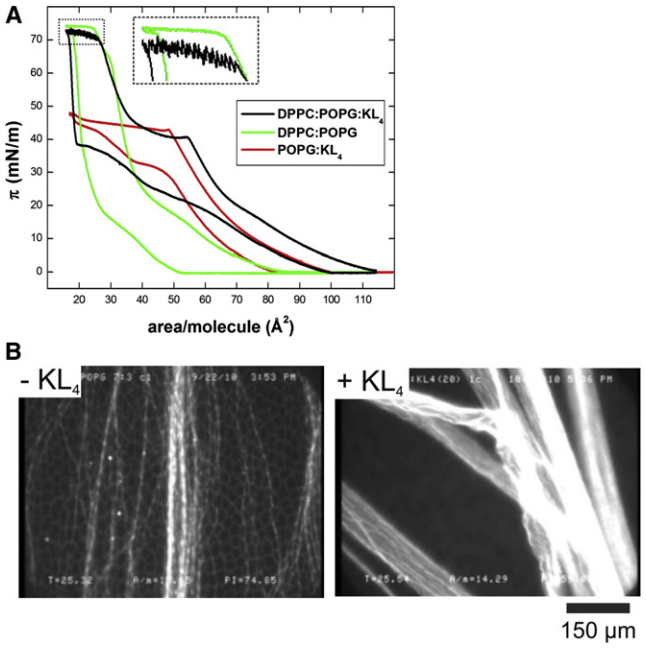

FIGURE 4 (*A*) Overlay of isotherms from one cycle of compression and expansion of POPG + 16 wt% KL_4 and DPPC/POPG (7:3) monolayers with a DPPC/POPG (7:3) + 16 wt% KL_4 monolayer support a mechanistic connection between the nano- and microscale material transformations taking place during compression of model lung surfactant (see text for details). Inset shows the increase in amplitude of π oscillations after addition of KL_4 during final collapse of the surfactant film induced by the increased fold size as shown in FM images in *B*.

Regardless of the specific mechanism, the demonstration that even a simple synthetic LS peptide like KL_4 is capable of generating nanosilo collapse structures that promote reversible monolayer folding supports the hypothesis that an underlying mechanistic connection exists between silos and monolayer folds. The value of elucidating a functional connection between these two monolayer structural transformations becomes apparent when considering the fact that the alveolar surface pressure during the breathing cycle remains in a regime above π ~50 mN/m (12), i.e., above the nanosilo plateau at π ~40 mN/m. Further studies with synthetic surfactants containing more advanced SP-B-mimicking peptides, such as Mini-B or Super

monolayers with 0, 4, 8, and 16 wt% KL_4 deposited onto solid mica substrates at π ~50 mN/m in a single compression experiment, showing an increase in number density, diameter, and height of nanosilos (*bright structures*). In AFM images of monolayers without peptide the condensed domains are brighter due to an increased height ~1 nm above the fluid matrix. Upon addition of KL_4, the condensed phases become hard to discern in AFM of monolayers based on lipid monolayer height contrast, due to the large height of the peptide-induced nanosilos in the fluid matrix. Accordingly, the location of condensed domains is revealed by areas where nanosilos are absent (see for example voids in nanosilo distribution in 8 wt% KL_4). (*F*) Section analysis of individual nanosilo indicated with box in *E*.

Mini-B, known to significantly improve LS function (21,26,33,38,39), could prove valuable by testing if nanosilos induced by such peptides establish stronger reversibly folding monolayers than observed here with KL_4.

In conclusion, we show that a simple synthetic LS peptide such as KL_4 is capable of generating nanosilo collapse structures in LS model films and thereby promote reversible folding and increase overall surfactant robustness in repeated compression-expansion cycles. We propose a new role for nanosilos in the structural transformations of LS films beyond their currently held function as surfactant repositories in additionally acting as triggers of reversible folding upon maximum compression. Combined with emerging knowledge of the fundamental relationship between monolayer mechanical properties and their folding dynamics (10,15), we believe that this hypothesis will prove helpful for the future design of physiologically functional synthetic lung surfactants.

The authors thank Dr. Luka Pocivavsek for invaluable discussions and insights on the manuscript.

This work was supported by March of Dimes (No. 6-FY07-357). K.Y.C.L. is grateful for the support of the US-Israel Binational Foundation (2006076). N.H.A. thanks the Danish Council for Independent Research, Natural Sciences for a Post-Doctoral Fellowship (No. 272-08-0087), and the University of Chicago Materials Research Science and Engineering Center (DMR 0820054) for the Kadanoff-Rice Postdoctoral Fellowship (2010-12). J.M.H. was supported by the National Science Foundation (MCB-0920316). R.H.N., F.J.W., and A.J.W. were supported by National Institutes of Health (NIH) RO1 HL-094641 and R44 HL-080775, and F.J.W. and A.J.W. were additionally supported by NIH RO1 ES-015330 and RO1 HL-092158.

REFERENCES

1. Daniels, C. B., S. Orgeig, and A. W. Smits. 1995. The evolution of the vertebrate pulmonary surfactant system. *Physiol. Zool.* 68:539–566.
2. Haagsman, H. P., and R. V. Diemel. 2001. Surfactant-associated proteins: functions and structural variation. *Comp. Biochem. Physiol. A Mol. Integr. Physiol.* 129:91–108.
3. Orgeig, S., P. S. Hiemstra, …, F. Possmayer. 2010. Recent advances in alveolar biology: evolution and function of alveolar proteins. *Respir. Physiol. Neurobiol.* 173 (*Suppl*):S43–S54.
4. Pattle, R. E. 1965. Surface lining of lung alveoli. *Physiol. Rev.* 45:48–79.
5. Clements, J. A., and D. F. Tierney. 1965. *In* Handbook of Physiology, Respiration, *Vol. 2.*; American Physiological Society, Bethesda, MD.
6. Notter, R. H. 2000. Lung Surfactants: Basic Science and Clinical Applications. Marcel Dekker, New York.
7. Power, J. H., I. R. Doyle, …, T. E. Nicholas. 1999. Ultrastructural and protein analysis of surfactant in the Australian lungfish *Neoceratodus forsteri:* evidence for conservation of composition for 300 million years. *J. Exp. Biol.* 202:2543–2550.
8. Pérez-Gil, J. 2008. Structure of pulmonary surfactant membranes and films: the role of proteins and lipid-protein interactions. *Biochim. Biophys. Acta.* 1778:1676–1695.
9. Alonso, C., T. Alig, …, J. A. Zasadzinski. 2004. More than a monolayer: relating lung surfactant structure and mechanics to composition. *Biophys. J.* 87:4188–4202.
10. Pocivavsek, L., S. L. Frey, …, K. Y. Lee. 2008. Lateral stress relaxation and collapse in lipid monolayers. *Soft Matter.* 4:2019–2029.
11. Ding, J., I. Doudevski, …, M. A. Sherman. 2003. Nanostructure changes in lung surfactant monolayers induced by interactions between palmitoyloleoylphosphatidylglycerol and surfactant protein B. *Langmuir.* 19:1539–1550.
12. Frey, S. L., L. Pocivavsek, …, K. Y. Lee. 2010. Functional importance of the NH2-terminal insertion sequence of lung surfactant protein B. *Am. J. Physiol. Lung Cell. Mol. Physiol.* 298:L335–L347.
13. Ding, J., D. Y. Takamoto, …, J. A. Zasadzinski. 2001. Effects of lung surfactant proteins, SP-B and SP-C, and palmitic acid on monolayer stability. *Biophys. J.* 80:2262–2272.
14. Lipp, M. M., K. Y. C. Lee, D. Y. Takamoto, J. A. Zasadzinski, and A. J. Waring. 1998. Coexistence of buckled and flat monolayers. *Phys. Rev. Lett.* 81:1650–1653.
15. Lee, K. Y. C. 2008. Collapse mechanisms of Langmuir monolayers. *Annu. Rev. Phys. Chem.* 59:771–791.
16. Diemel, R. V., M. M. Snel, …, J. J. Batenburg. 2002. Multilayer formation upon compression of surfactant monolayers depends on protein concentration as well as lipid composition. An atomic force microscopy study. *J. Biol. Chem.* 277:21179–21188.
17. Krol, S., M. Ross, …, A. Janshoff. 2000. Formation of three-dimensional protein-lipid aggregates in monolayer films induced by surfactant protein B. *Biophys. J.* 79:904–918.
18. Nogee, L. M., G. Garnier, …, H. R. Colten. 1994. A mutation in the surfactant protein B gene responsible for fatal neonatal respiratory disease in multiple kindreds. *J. Clin. Invest.* 93:1860–1863.
19. Clark, J. C., S. E. Wert, …, J. A. Whitsett. 1995. Targeted disruption of the surfactant protein B gene disrupts surfactant homeostasis, causing respiratory failure in newborn mice. *Proc. Natl. Acad. Sci. USA.* 92:7794–7798.
20. Moya, F., and A. Maturana. 2007. Animal-derived surfactants versus past and current synthetic surfactants: current status. *Clin. Perinatol.* 34:145–177, viii.
21. Notter, R. H., A. L. Schwan, …, A. J. Waring. 2007. Novel phospholipase-resistant lipid/peptide synthetic lung surfactants. *Mini Rev. Med. Chem.* 7:932–944.
22. Cochrane, C. G., and S. D. Revak. 1991. Pulmonary surfactant protein B (SP-B): structure-function relationships. *Science* 254:566–568.
23. Mansour, H. M., S. Damodaran, and G. Zografi. 2008. Characterization of the in situ structural and interfacial properties of the cationic hydrophobic heteropolypeptide, KL4, in lung surfactant bilayer and monolayer models at the air-water interface: implications for pulmonary surfactant delivery. *Mol. Pharm.* 5:681–695.
24. Saleem, M., M. C. Meyer, …, H. J. Galla. 2008. The surfactant peptide KL4 in lipid monolayers: phase behavior, topography, and chemical distribution. *J. Biol. Chem.* 283:5195–5207.
25. Fields, C. G., D. H. Lloyd, …, R. L. Noble. 1991. HBTU activation for automated Fmoc solid-phase peptide synthesis. *Pept. Res.* 4:95–101.
26. Waring, A. J., F. J. Walther, …, J. A. Zasadzinski. 2005. The role of charged amphipathic helices in the structure and function of surfactant protein B. *J. Pept. Res.* 66:364–374.
27. Lee, K. Y. C., M. M. Lipp, …, A. J. Waring. 1998. Apparatus for the continuous monitoring of surface morphology via fluorescence microscopy during monolayer transfer to substrates. *Langmuir.* 14:2567–2572.
28. Gopal, A., and K. Y. C. Lee. 2001. Morphology and collapse transitions in binary phospholipid monolayers. *J. Phys. Chem. B.* 105:10348–10354.
29. Fleming, B. D., and K. M. W. Keough. 1988. Surface respreading after collapse of monolayers containing major lipids of pulmonary surfactant. *Chem. Phys. Lipids.* 49:81–86.
30. Long, J. R., F. D. Miles, O. K. Ganesh, V. C. Antharam, and R. S. Farver. 2010. Partitioning, dynamics, and orientation of lung surfactant peptide KL4 in phospholipid bilayers. *Biochim. Biophys. Acta.* 1798:216–222.

31. Walther, F. J., J. Hernández-Juviel, …, A. J. Waring. 1998. Protein composition of synthetic surfactant affects gas exchange in surfactant-deficient rats. *Pediatr. Res.* 43:666–673.

32. Nilsson, G., M. Gustafsson, …, J. Johansson. 1998. Synthetic peptide-containing surfactants—evaluation of transmembrane versus amphipathic helices and surfactant protein C poly-valyl to poly-leucyl substitution. *Eur. J. Biochem.* 255:116–124.

33. Walther, F. J., A. J. Waring, …, R. H. Notter. 2010. Critical structural and functional roles for the N-terminal insertion sequence in surfactant protein B analogs. *PLoS ONE.* 5:e8672.

34. Serrano, A. G., M. Ryan, …, J. Pérez-Gil. 2006. Critical structure-function determinants within the N-terminal region of pulmonary surfactant protein SP-B. *Biophys. J.* 90:238–249.

35. Shanmukh, S., N. Biswas, …, R. A. Dluhy. 2005. Structure and properties of phospholipid-peptide monolayers containing monomeric SP-B(1–25) II. Peptide conformation by infrared spectroscopy. *Biophys. Chem.* 113:233–244.

36. Pocivavsek, L., B. Leahy, …, E. Cerda. 2009. Geometric tools for complex interfaces: from lung surfactant to the mussel byssus. *Soft Matter* 5:1963–1968.

37. Veldhuizen, E. J. A., J. J. Batenburg, …, H. P. Haagsman. 2000. The role of surfactant proteins in DPPC enrichment of surface films. *Biophys. J.* 79:3164–3171.

38. Walther, F. J., A. J. Waring, …, R. H. Notter. 2007. Dynamic surface activity of a fully synthetic phospholipase-resistant lipid/peptide lung surfactant. *PLoS ONE.* 2:e1039.

39. Mingarro, I., D. Lukovic, …, J. Pérez-Gil. 2008. Synthetic pulmonary surfactant preparations: new developments and future trends. *Curr. Med. Chem.* 15:393–403.